J. Ocean Univ. China (Oceanic and Coastal Sea Research)
https://doi.org/10.1007/s11802-023-5228-y
ISSN 1672-5182, 2023 22 (3): 637-648
http://www.ouc.edu.cn/xbywb/
E-mail:xbywb@ouc.edu.cn

An Innovative Approach to Predicting Scour Depth Around Foundations Under Combined Waves and Currents in Large-Scale Tests Based on Small-Scale Tests

HU Ruigeng[1)], LIU Hongjun[1), 2), 3), *], LU Yao[1)], WANG Xiuhai[1), 3)], and SHI Wei[4)]

1) *College of Environmental Science and Engineering*, *Ocean University of China*, *Qingdao* 266100, *China*
2) *Key Laboratory of Marine Environment and Ecology*, *Ministry of Education*, *Qingdao* 266100, *China*
3) *Shandong Provincial Key Laboratory of Marine Environment and Geological Engineering*, *Qingdao* 266100, *China*
4) *School of Civil Engineering*, *Qingdao University of Technology*, *Qingdao* 266033, *China*

(Received October 11, 2021; revised November 29, 2021; accepted December 16, 2021)

Abstract This study presents an innovative theoretical approach to predicting the scour depth around a foundation in large-scale model tests based on small-scale model tests under combined waves and currents. In the present approach, the hydrodynamic parameters were designed based on the Froude similitude criteria. To avoid the cohesive behavior, we scaled the sediment size based on the settling velocity similarity, *i.e.*, the suspended load similarity. Then, a series of different scale model tests was conducted to obtain the scour depth around the pile in combined waves and currents. The fitting formula of scour depth from the small-scale model tests was used to predict the results of large-scale tests. The accuracy of the present approach was validated by comparing the prediction values with experimental data of large-scale tests. Moreover, the correctness and accuracy of the present approach for foundations with complex shapes, *e.g.*, the tripod foundation, was further checked. The results indicated that the fitting line from small-scale model tests slightly overestimated the experimental data of large-scale model tests, and the errors can be accepted. In general, the present approach was applied to predict the maximum or equilibrium scour depth of the large-scale model tests around single piles and tripods.

Key words scour; scour depth prediction; Froude similarity; scale effects; combined waves and currents

1 Introduction

As a kind of clean energy, offshore wind energy has been developed rapidly in recent years. Offshore wind energies reduce greenhouse emissions efficiently, contributing to addressing the climate change challenges. Considering the cost-effective and easy installation procedure, monopiles are now generally used as foundations of offshore wind turbines. After the installation of monopiles in the ocean environment, the seabed in the vicinity of monopile suffers from scour under the action of waves and currents (Sumer *et al.*, 1992, 1997; Sumer and Fredsøe, 2001). As a result, scour holes emerge around monopiles. Scour holes decrease the embedded depth of the foundation and weaken its bearing capacity (Li *et al.*, 2018; Fazeres-Ferradosa *et al.*, 2019, 2021). As a result, the scour evolution and scour depth prediction around monopiles have caught great attention from coastal engineers.

The horseshoe and wake vortexes significantly contribute to the development of scour holes around foundations (Sumer *et al.*, 1992, 1997; Sumer and Fredsøe, 2001; Petersen *et al.*, 2012; Schendel *et al.*, 2020). The horseshoe vortex is mainly related to the *KC* number, pile Reynold number Re_d, and dimensionless boundary layer thickness δ/D under combined waves and currents (Sumer and Fredsøe, 2001; Roulund *et al.*, 2005; Corvaro *et al.*, 2018). The *KC* indicates the ratio of the displacement amplitude of water particles in one wave cycle to the pile diameter. Thus, a small *KC* reflects a small displacement amplitude. The boundary layer cannot be separated from the seabed in small *KC* conditions, resulting in the difficult formation of the horseshoe vortex. Sumer *et al.* (1992) conducted a series of flume tests to investigate the scour evolution around a single pile, indicating that scour occurred when $KC>6$, and the high *KC* resulted in large scour depths. The phenomenon can be attributed to the increase in lifespan and scale of the horseshoe vortex with the increase in *KC*. The boundary layer thickness δ has a huge influence on the boundary layer separation and horseshoe vortex formation (Roulund *et al.*, 2005). The smaller value of δ/D, the smaller scale of the horseshoe vortex. No horseshoe vortex formed when $\delta/D<$O (0.01). The Re_d affects the flow regime in the boundary layer. The laminar flow

* Corresponding author. E-mail: hongjun@ouc.edu.cn

prevails in the boundary layer when Re_d<500, indicating that the boundary layer is difficult to separate from the seabed due to the relatively high viscous force of laminar flow (Roulund *et al.*, 2005; Tavouktsoglou *et al.*, 2017). The turbulent flow rose up when Re_d>500, instructing the increased momentum exchange between the turbulent and external boundary layers, which contributed to the separation of the boundary layer from seabed; however, an extremely high Re_d can cause the location of the separation point of wake vortex at the two pile sides to transfer downstream, leading to a narrow wake vortex field (Sumer *et al.*, 1992, 1997; Roulund *et al.*, 2005). Tavouktsoglou *et al.* (2017) investigated the effects of Re_d on the equilibrium scour depth around the pile, and the findings of the equilibrium scour depth decreased with the increase in the Re_d when $10^3 < Re_d < 4\times10^6$. According to Ettema *et al.* (1998) and Corvaro *et al.* (2018), the influence of Re_d can be ignored when it is a fully turbulent flow around a pile; the condition of fully turbulent flow in laboratory flume tests is difficult to achieve.

Thus far, scour evolution around single piles has been studied generally in waves and currents through laboratory flume experiments, and numerous scour depth prediction formulas have been developed based on quantitative small-scale flume experimental data (Sumer *et al.*, 1992; Sumer and Fredsøe, 2001; Qi and Gao, 2014; Corvaro *et al.*, 2018). In laboratory tests on scour evolution, the hydrodynamic parameters were usually designed in accordance with the Froude similitude criteria (Arboleda Chavez *et al.*, 2019; Wu *et al.*, 2020). However, guaranteeing the rigorous similarity of all parameters between the model and prototype is impossible, which results in the scale effects of the model tests (Schendel *et al.*, 2018; Hu *et al.*, 2021). For example, the bed sediment size is usually scaled geometrically based on a model scale to avoid the interparticle cohesive forces. As a result, the relatively large-scale sediment sizes may lead to the underestimation of suspended load transport and overestimation of bedload transport compared with field conditions. In addition, the distorted scaled sediment may cause the error of bed roughness between the model and prototype and thus shows large effects for boundary layer thickness and scour evolution (Lee and Sturm, 2009). Wu *et al.* (2020) carried out a number of large-scale wave flume tests to investigate the scour development around piles in waves and currents, indicating that the existing scour depth prediction approaches are conservative when applied to large-scale tests; thus, the scale effects for scour depth prediction must be studied further.

Huang *et al.* (2009) investigated the scale effects on the flow field and scour evolution around large bridge piers using a numerical model. Full- and small-scale numerical models based on Froude similitude criteria were built in their study, and the results indicated that the small-scale model with Froude similarity can cause errors when utilized to predict the scour depth of the prototype. As described above, when the hydrodynamic parameters are designed based on Froude similarity, the discrepancy between the model and prototype can be attributed to distorted scaled sediments. Typically, compared with the requested sediment size by geometric similarity, relatively large-sized soil particles were used in laboratory flume tests to avoid interparticle cohesive forces; thus, the results from scour depth prediction formulas predominantly based on small-scale tests will have a gap with the measured data in the field (Ettema *et al.*, 1998; Lee and Sturm, 2009). In addition, compared with the prototype, the choice of sediment size in model tests usually distorts the ratio of pile diameter to sediment size, resulting in a large scour depth around the pile in model tests. According to the experimental results of Huang *et al.* (2009) and Lee and Sturm (2009), the model distortion due to sediment size is also related to the scale and intensity of horseshoe vortex at upstream pier edges. Wang *et al.* (2013) proposed a theoretical formula to obtain the prototype scour depth around a pile by conducting a series of small-scale model tests. In the experiments, the prototype or scaled sediments were used in model tests, and the size of sediments was selected based on the bedload similarity. Notably, the theoretical formula was derived and verified under the condition of steady currents. Thus, the adaptation and accuracy for the condition of combining waves and currents must be validated further.

In general, scale effects exist when the similarity criteria cannot be satisfied completely between the prototype and model. The discrepancy from scale effects may be reduced efficiently by conducting experiments in a sufficiently large flume. However, the installation cost, experimental setup, and technique may be limited for extremely large-scale model tests. Therefore, an innovative theoretical approach was proposed in this study to predict the scour depth around foundations in large-scale model tests based on small-scale model tests under combined waves and currents. In the present approach, the hydrodynamic parameters were designed based on Froude similitude criteria. To avoid the cohesive behavior, we scaled the sediment size based on the settling velocity similarity, *i.e.*, the suspended load similarity. Then, a series of different scale model tests was conducted to obtain the scour depth around a pile in combining waves and currents. The fitting formula of scour depth from small-scale model tests was used to predict the results of large-scale tests. The accuracy of the present approach was validated by comparing the prediction values with experimental data from large-scale tests. Moreover, the adaptation of the present approach for foundations with complex shapes, *e.g.*, the tripod foundation, was further checked. Finally, the merits and disadvantages of the present approach were evaluated in the Discussion section.

2 Theoretical Approach

2.1 Scale Law

The hydrodynamic parameters corresponded to the Froude similarity criteria from the prototype to the model, including flow model scaling, wave model scaling, and sediment transport scaling (Ettema *et al.*, 1998; Huang and Xu, 2008).

1) Flow model scaling

The flow follows the continuity equation, Froude similarity criteria, and bed roughness similarity criteria. Suppose that λ stands for the scale ratio of the prototype value to the model value. The λ_h and λ_l are the geometric scale ratio in vertical and horizontal directions, respectively. In the present study, the same geometric scales in vertical and horizontal directions were adopted, that is, $\lambda_h=\lambda_l$. The flow velocity scale ratio λ_u, Manning roughness scale ratio λ_n, and scour time scale ratio λ_t are respectively given by the following (Ettema *et al.*, 1998; Huang and Xu, 2008):

$$\lambda_u=\lambda_h^{1/2}, \quad (1)$$

$$\lambda_n=\lambda_h^{1/6}, \quad (2)$$

$$\lambda_t=\frac{\lambda_l}{\lambda_u}=\lambda_h^{1/2}. \quad (3)$$

2) Wave model scaling

The wave parameters were scaled using the following relationships (Huang and Xu, 2008; Zhang and Jin, 2017)

$$\lambda_L=\lambda_H=\lambda_h, \quad (4)$$

$$\lambda_T=\lambda_h^{1/2}, \quad (5)$$

where λ_L is the wavelength scale ratio, λ_H is the wave height scale ratio, and λ_T is the wave period scale ratio.

3) Sediment transport scaling

The sediment motion can be classified into bedload and suspended load transport under combined waves and currents. Ensuring the bedload and suspended load similarity simultaneously is typically impossible; however, the model should have the same dominant sediment transport mode as the prototype (Sutherland and Whitehouse, 1998). The hydrodynamics parameters in the present model tests (Section 3.1) were referred to the environmental conditions of the BZ1 offshore wind farm, which is located in the Yellow River Delta of China. According to Jia *et al.* (2020), the suspended load transport is likely to prevail in that location; thus, the sediment size was scaled based on the suspended load transport similarity. The suspended load transport similarity was mainly ensured using the settling velocity similarity. The settling velocity scale ratio λ_w is given by the equation below (Huang and Xu, 2008):

$$\lambda_w=\lambda_u\frac{\lambda_h}{\lambda_l}=\lambda_u. \quad (6)$$

2.2 Derivation of the Theoretical Approach

The sediment motion continuity equation is expressed as follows (Zhao and Xu, 2009):

$$\frac{\partial S}{\partial t}+\frac{\partial q}{\partial r}=0, \quad (7)$$

where S is the scour depth, t denotes the scour time, q refers to the sediment volumetric transport rate, and r corresponds to the maximum distance of sediment transportation.

Eq. (7) can be recast into finite difference format:

$$\frac{\Delta S}{\Delta t}=-\frac{\Delta q}{\Delta r}, \quad (8)$$

$$\Delta S=-\frac{\Delta q}{\Delta r}\Delta t. \quad (9)$$

When S_t is the maximum scour depth in $0-t$, r_t denotes the maximum distance of sediments transportation in $0-t$, and q_t indicates the maximum sediment volumetric transport rate in $0-t$, Eq. (9) can be written in the following form:

$$S_t=-\frac{q_t}{r_t}t. \quad (10)$$

According to Engelund and Hansen (1967), the equation of total sediment transport rate can be expressed by the following:

$$q_t=\frac{0.05u^2\rho^{1/2}d_{50}^{1/2}}{(\rho_s-\rho)^{1/2}g^{1/2}}\left[\frac{\tau_c}{(\rho_s-\rho)gd_{50}}\right]^{3/2}, \quad (11)$$

where u is the flow velocity, ρ represents the water density, ρ_s refers to the sediment density, d_{50} stands for the sediment median diameter, g denotes the gravity acceleration, and τ_c is the shear stress on the seabed induced by steady currents.

According to Zhou (2009), τ_c can be calculated as follows:

$$\tau_c=\rho C_D u^2, \quad (12)$$

$$C_D=\frac{g}{C_h^2}, \quad (13)$$

where C_D is the friction coefficient under steady currents, and C_h denotes the Chezy coefficient.

Substituting Eqs. (12) and (13) into Eq. (11) yields the following.

$$q_t=\frac{0.05C_h u\tau_c^2}{g^{5/2}\rho^2\left(\frac{\rho_s}{\rho}-1\right)^2 d_{50}}. \quad (14)$$

In Eq. (14), τ_c should be replaced by the shear stress τ_{wc} on the seabed induced by waves and currents when it is applied for the condition of combined waves and currents. Li (2016) demonstrated that τ_{wc} can be expressed by the following:

$$\tau_{wc}=\frac{1}{2}\rho f_{wc}u_{wa}^2, \quad (15)$$

where f_{wc} is the friction coefficient under combined waves and currents, and u_{wa} denotes the amplitude velocity of the undisturbed wave-induced oscillatory flow above the wave boundary layer.

Simons *et al.* (2001) proposed the following equations for the f_{wc}:

$$f_{wc} = k\left(\frac{a_p}{d_{50}}\right)^m , \tag{16}$$

$$a_p = \frac{u_{wa}T}{2\pi} , \tag{17}$$

where k and m are coefficients that can be obtained by laboratory flume experiments. a_p is the wave orbital diameter above the wave boundary layer.

Substituting Eqs. (15–17) into Eq. (14) yields the following:

$$q_t = C_1 \cdot \frac{C_h u \rho^2 T^{2m} u_{wa}^{2m+4}}{(2\pi)^{2m} g^{5/2} (\rho_s - \rho)^2 d_{50}^{2m+1}} , \tag{18}$$

where C_1 is the constant.

Le Roux (2001) derived the following equations to determine u_{wa} by the settling velocity ω:

$$u_{wa} = \frac{\theta_{cr} g d_{50} (\rho_s - \rho) \rho^{1/2} \mu^{1/2}}{\pi^{1/2} T^{1/2}} , \tag{19}$$

$$\theta_{cr} = 0.0246 \omega_d^{-0.55} , \tag{20}$$

$$\omega_d = \omega \left[\frac{\rho^2}{\mu g(\rho_s - \rho)}\right]^{1/3} , \tag{21}$$

where ω_d refers to the dimensionless settling velocity, μ denotes the water dynamic viscosity, and θ_{cr} is the critical Shields parameter.

Substituting Eqs. (19–21) into Eq. (18) yields the following:

$$q_t = C_2 C_h u d_{50}^3 \pi^m T^{m-2} \rho^{\frac{68}{15}+\frac{4m}{15}} \omega^{-\left(\frac{11}{5}+\frac{11m}{10}\right)} \cdot \mu^{\frac{41}{15}+\frac{41m}{30}} g^{\frac{67}{30}+\frac{71m}{30}} (\rho_s - \rho)^{\frac{41}{15}+\frac{71m}{30}} , \tag{22}$$

where C_2 is a constant.

The scale ratio of the maximum sediment volumetric transport rate λ_{q_t} can be written as follows:

$$\lambda_{q_t} = C_3 \lambda_{C_h} \lambda_u \lambda_{d_{50}}^3 \lambda_T^{m-2} \lambda_\rho^{\frac{68}{15}+\frac{4m}{15}} \lambda_\omega^{-\left(\frac{11}{5}+\frac{11m}{10}\right)} \cdot \lambda_\mu^{\frac{41}{15}+\frac{41m}{30}} \lambda_g^{\frac{67}{30}+\frac{71m}{30}} \lambda_{\rho_s-\rho}^{\frac{41}{15}+\frac{71m}{30}} , \tag{23}$$

where C_3 is a constant. When the fluid between the prototype and model are the same, the $\lambda_\rho=1$, $\lambda_\mu=1$, and $\lambda_g=1$. In this way, Eq. (23) can be simplified as follows:

$$\lambda_{q_t} = C_3 \lambda_{C_h} \lambda_u \lambda_{d_{50}}^3 \lambda_T^{m-2} \lambda_\omega^{-\left(\frac{11}{5}+\frac{11m}{10}\right)} \lambda_{\rho_s-\rho}^{\frac{41}{15}+\frac{71m}{30}} . \tag{24}$$

The Chezy coefficient C_h in Eq. (13) can be calculated by the Manning formula (Huang and Xu, 2008)

$$C_h = \frac{1}{n} R^{1/6} , \tag{25}$$

where n is the roughness coefficient, and R is the hydraulic radius.

The roughness scale ratio λ_n was calculated in accordance with Eq. (2); thus, the Chezy coefficient scale ratio λ_{C_h} can be calculated by the following:

$$\lambda_{C_h} = \frac{\lambda_R^{1/6}}{\lambda_n} = \frac{\lambda_h^{1/6}}{\lambda_h^{1/6}} = 1 . \tag{26}$$

Substituting Eqs. (1), (5), (6), and (26) into Eq. (24) can be simplified as follows:

$$\lambda_{q_t} = C_3 \lambda_{d_{50}}^3 \lambda_h^{-\left(\frac{m}{20}+\frac{8}{5}\right)} \lambda_{\rho_s-\rho}^{\frac{41}{15}+\frac{71m}{30}} . \tag{27}$$

Based on Eq. (10), the maximum scour depth scale ratio λ_{S_t} is given by the following:

$$\lambda_{S_t} = -\frac{\lambda_{q_t}}{\lambda_{r_t}} \lambda_t . \tag{28}$$

Substitution of Eqs. (3) and (27) into Eq. (28) yields the following:

$$\lambda_{S_t} = C_4 \lambda_{d_{50}}^3 \lambda_h^{-\left(\frac{m}{20}+\frac{21}{10}\right)} \lambda_{\rho_s-\rho}^{\frac{41}{15}+\frac{71m}{30}} , \tag{29}$$

where C_4 is the constant.

Supposing that S_{tp} and S_{tm} stand for the maximum scour depth in prototype and model, respectively, Eq. (29) can be written as follows:

$$S_{tm} = C_5 \lambda_{d_{50}}^{-3} \lambda_h^{\frac{m}{20}+\frac{27}{20}} \lambda_{\rho_s-\rho}^{-\left(\frac{41}{15}+\frac{71m}{30}\right)} S_{tp} , \tag{30}$$

where C_5 is the constant.

Performing the logarithmic calculations for Eq. (30) yields the following:

$$\log S_{tm} = C_6 + 3\log \lambda_{d_{50}} - \left(\frac{m}{20}+\frac{27}{20}\right)\log \lambda_h + \left(\frac{41}{15}+\frac{71m}{30}\right)\log \lambda_{\rho_s-\rho} , \tag{31}$$

where C_6 is the constant.

Scaling the sediment median diameter d_{50} based on geometric similarity, *i.e.*, $\lambda_{d_{50}}=\lambda_h$, leads to a very small model sediment size exhibiting a cohesive behavior (Ettma *et al.*, 1998; Lee and Sturm, 2009; Schendel *et al.*, 2018). Moreover, preparing materials with very small particle sizes for small-scale model tests is difficult. A new approach was proposed to select the sediment size in model tests. In the present approach, the sediment size was scaled based on the settling velocity similarity, *i.e.*, the suspended load similarity. The only difference of bed materials between the prototype and model is d_{50}; thus, $\lambda_{\rho_s-\rho} \approx 1$. In this manner, Eq. (31) is further simplified to the following:

$$\log S_{tm} = C_6 + 3\log \lambda_{d_{50}} - \left(\frac{m}{20} + \frac{27}{20}\right)\log \lambda_h . \quad (32)$$

Based on Zhou (2009), the settling velocity can be calculated by Stokes formula:

$$\omega = \frac{1}{18}\frac{\rho_s - \rho}{\rho} g \frac{d_{50}^2}{\upsilon}, \quad (33)$$

where υ is the viscosity coefficient of water.

The following relationship for determining the scale ratio of d_{50} was deduced using Eqs. (1), (6), and (33):

$$\lambda_{d_{50}} = \lambda_h^{1/4} . \quad (34)$$

Substituting Eq. (34) into Eq. (32) yields the following:

$$\log S_{tm} = C_6 - \left(\frac{m}{20} + \frac{27}{20}\right)\log \lambda_h . \quad (35)$$

According to Eq. (35), a series of different scale model tests was conducted to obtain the S_{tm} around foundations under combined waves and currents. Then, the experimental data were plotted in $\log h_e \sim \log \lambda_h$ coordinate. Afterward, the data of the small-scale model tests were fitted, and the fitting line was extended. In this way, the S_{tm} of large-scale model tests can be obtained by extrapolating the fitting line of small-scale model tests.

3 Experimental Design

3.1 Scour Tests Around a Single Pile

The experiments were carried out in a wave and current flume (Fig.1, length: 20 m; width: 1.0 m; and 1.2 m in height). The soil pit (length: 3.0 m and height: 0.4 m) was set at the center and lower portion of the flume. The wave generation system was installed at the offshore side of the wave flume, respectively, and it consisted of the double-piston wave paddle, piston rod, and electric control cabinet. Two axial-flow pumps were installed at the offshore and onshore sides of the wave flume. The gravels were placed at the onshore side of the flume as the wave absorption band (2 m in length, 14° in inclination). The hydrodynamics parameters referred to the environmental conditions of the BZ1 offshore wind farm, which is located in the Yellow River Delta of China. The waves and currents parameters in a 5-year return period were as follows: wave height $H = 5.8$ m, wavelength $L = 80$ m, wave period $T = 8$ s, water depth $h = 10$ m, and current velocity $U_c = 1.5$ m s^{-1}. The monopiles (diameter $D = 4$ m) were used as the foundations in the BZ1 offshore wind farm. The prototype sediment was medium sand, and the basic mechanical parameters of the sand samples were as follows: median diameter $d_{50} = 0.386$ mm, specific gravity of soil particle $G_s = 2.72$, maximum void ratio $e_{\max} = 1.2$, minimum void ratio $e_{\min} = 0.54$, permeability coefficient $k_s = 1.5 \times 10^{-5}$ m s^{-1}, Poisson's ratio $\nu = 0.28$, porosity $n = 0.42$, and shear modulus $G = 5.8 \times 10^5$ Pa. Fourteen groups of different scale scour model tests were conducted in the wave-current flume, and the geometric scale λ_h ranged from 25 to 90. As discussed in Section 2, the hydrodynamic parameters in model tests (Table 1) were designed in accordance with the Froude similarity criteria. The sediment size was scaled based on the settling velocity similarity, *i.e.*, the suspended load similarity. Fig.2 shows the sediment size grading curves. Supposing that the scour time t in the prototype was 72 h, the scour time in different scale model tests was ensured by Eq. (3). The single pile model was installed at the center of the soil pit. As shown in Fig.1, the scour depth measuring positions were set around the pile model. The echo sounder was used to measure the real-time scour depth evolution. The wave height gage was installed on the upstream section between the pile model and wave paddle. An acoustic Doppler velocimeter was adopted to measure the flow velocity in tests. Table 1 lists the test plans and several specified experimental parameters.

3.2 Scour Tests Around a Tripod

To further validate the adaptation of the present theoretical approach for foundations with complex shapes, we carried out scour tests around tripods in combining waves and currents. Fig.3 illustrates the schematic of the tripod model, which was manufactured by 3D printing technology. The tripod model was installed at the center of the soil pit with three installation angles $\alpha = 0°$, 90°, 180°. As shown in Fig.4, angles $\alpha = 0°$ and $\alpha = 180°$ mean that one

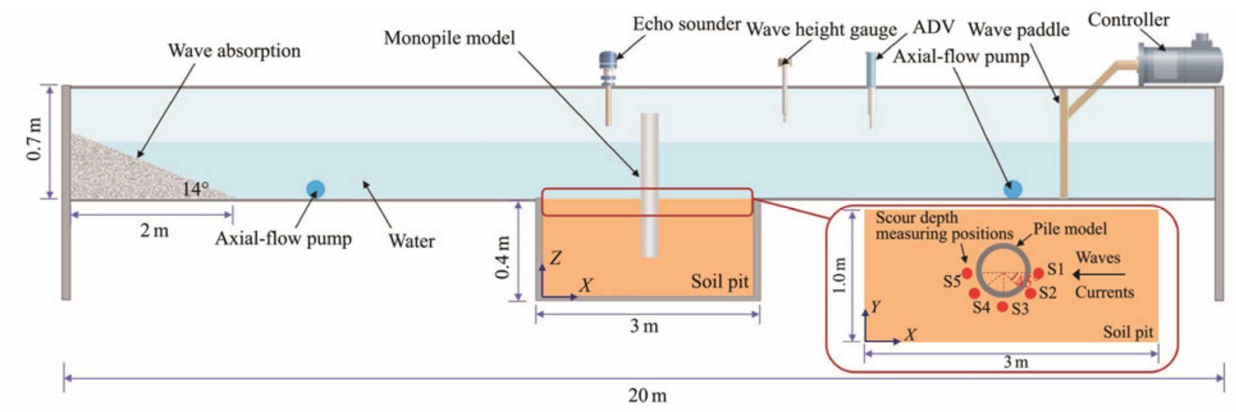

Fig.1 Sketch of the experimental setup.

Table 1 Test plans and parameters for single piles

Case	λ_h	D (cm)	U_c (cm s^{-1})	L (cm)	H_w (cm)	T (s)	H (cm)	d_{50} (mm)	T (min)	θ	F_r	Re_d ($\times10^4$)	S_{max}/D	Sand type
R1	90	4.4	15.8	88	6.4	0.84	11.1	0.125	455	0.55	0.33	0.82	0.78	Sand 1
R2	85	4.7	16.3	94	6.8	0.86	11.8	0.127	468	0.56	0.34	0.89	0.81	Sand 2
R3	80	5.0	16.8	100	7.3	0.89	12.5	0.129	482	0.57	0.35	0.97	0.82	Sand 3
R4	75	5.3	17.3	106	7.7	0.92	13.3	0.131	498	0.59	0.36	1.07	0.86	Sand 4
R5	70	5.7	17.9	114	8.3	0.95	14.3	0.133	516	0.61	0.37	1.19	0.92	Sand 5
R6	65	6.1	18.6	123	8.9	0.99	15.4	0.136	535	0.63	0.39	1.33	0.93	Sand 6
R7	60	6.6	19.4	133	9.7	1.03	16.7	0.139	557	0.66	0.40	1.50	0.96	Sand 7
R8	55	7.2	20.2	145	10.5	1.07	18.2	0.142	582	0.68	0.42	1.71	1.01	Sand 8
R9	50	8.0	21.2	160	11.6	1.13	20.0	0.145	610	0.71	0.44	1.97	1.04	Sand 9
R10	45	8.8	22.4	177	12.9	1.19	22.2	0.149	643	0.75	0.47	2.31	1.11	Sand 10
R11	40	10.0	23.7	200	14.5	1.26	25.0	0.153	683	0.79	0.50	2.76	1.12	Sand 11
R12	35	11.4	25.4	228	16.6	1.35	28.6	0.159	730	0.84	0.53	3.37	1.18	Sand 12
R13	30	13.3	27.4	266	19.3	1.46	33.3	0.165	788	0.91	0.57	4.25	1.23	Sand 13
R14	25	16.0	30.0	320	23.2	1.60	40.0	0.173	864	0.99	0.63	5.59	1.32	Sand 14

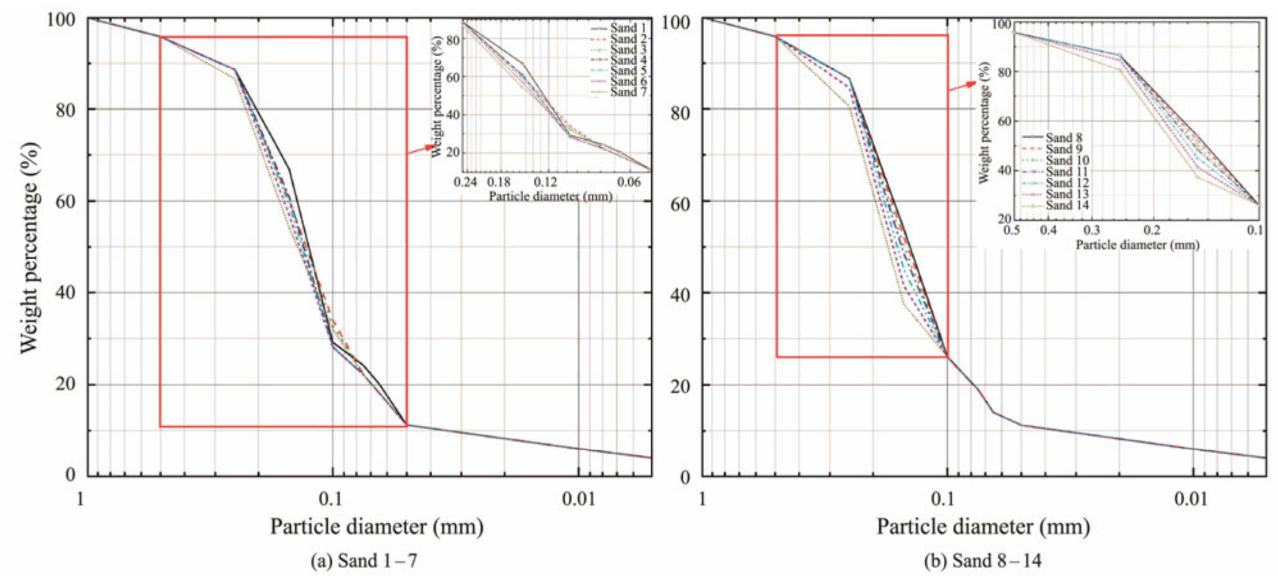

Fig.2 Particle size grading curves of the soil samples.

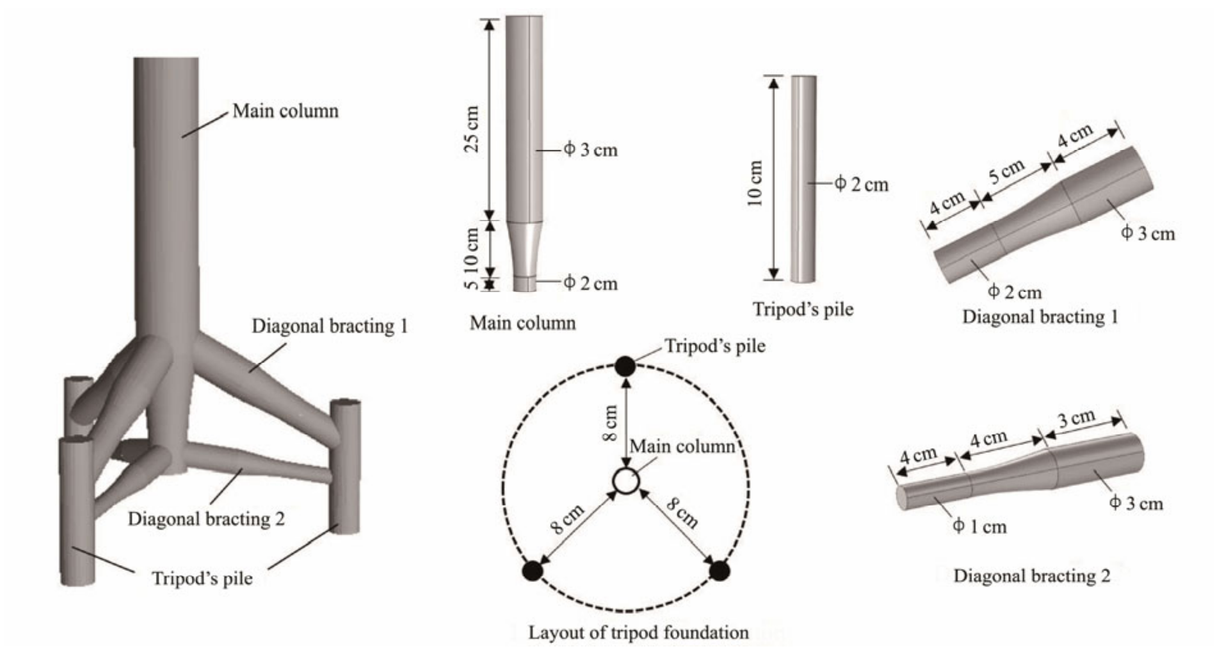

Fig.3 Schematic of the tripod model.

and two piles faced the incoming waves, respectively, and $\alpha=90^\circ$ means asymmetric installation. Nine groups of different scale scour model tests were conducted in the wave-current flume, and the geometric scale λ_h ranged from 30 to 90. The hydrodynamics and sediment parameters were the same as those described in Section 3.1, and the discussion will not be repeated here. Table 2 lists the test plans and several specified experimental parameters. As shown in Fig.4, the scour depth measuring positions were set in front of the pile, rear pile, and under the column.

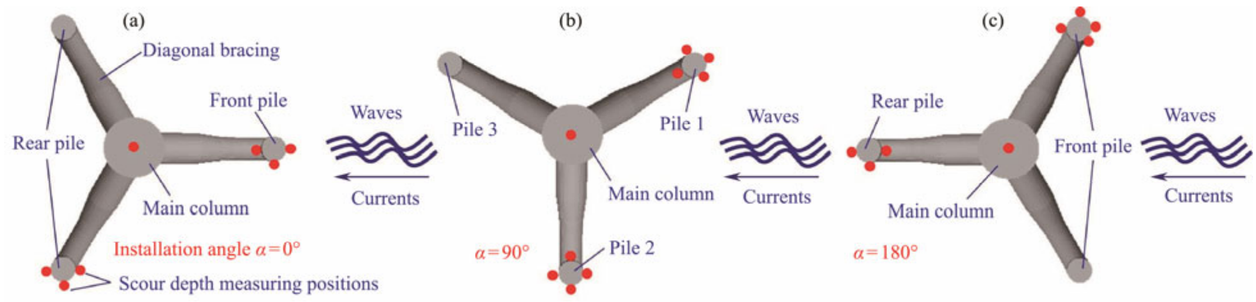

Fig.4 Sketch of tripod installation in wave-current flume: (a) $\alpha=0^\circ$, (b) $\alpha=90^\circ$, and (c) $\alpha=180^\circ$.

Table 2 Test plans and parameters for tripod

Case	λ_h	U_c (cm s^{-1})	L (cm)	H_w (cm)	T (s)	H (cm)	d_{50} (mm)	T (min)	θ	F_r	Re_d ($\times10^4$)	Sand type	$S_{m,\max}/D_m$		
													0°	90°	180°
R15	90	15.8	88	6.4	0.84	11.1	0.125	455	2.11	0.33	0.49	Sand 1	0.93	1.02	0.85
R16	80	16.8	100	7.3	0.89	12.5	0.129	482	0.57	0.35	0.58	Sand 3	0.96	1.06	0.90
R17	70	17.9	114	8.3	0.95	14.3	0.133	516	0.61	0.37	0.71	Sand 5	1.02	1.12	0.95
R18	60	19.4	133	9.7	1.03	16.7	0.139	557	0.65	0.40	0.90	Sand 7	1.14	1.26	1.08
R19	50	21.2	160	11.6	1.13	20.0	0.145	610	0.71	0.44	1.18	Sand 9	1.16	1.30	1.10
R20	45	22.4	177	12.9	1.19	22.2	0.149	643	0.75	0.47	1.38	Sand 10	1.20	1.32	1.12
R21	40	23.7	200	14.5	1.26	25.0	0.153	683	0.79	0.50	1.65	Sand 11	1.21	1.33	1.13
R22	35	25.4	228	16.6	1.35	28.6	0.159	730	0.84	0.53	2.02	Sand 12	1.23	1.34	1.15
R23	30	27.4	266	0.19	1.46	0.33	0.165	788	0.91	0.57	2.55	Sand 13	1.24	1.36	1.19

Note: D_m, the diameter of the main column (see Fig.3).

4 Experimental Results

4.1 Single Pile

1) Scour evolution and scour morphology

Fig.5 depicts the scour evolution curves of cases R2, R6, R8, and R12 at position S2 (Fig.1). As shown in Fig.5, the scour depth developed rapidly at the initial stage, and the scour rate slowed down. Finally, the curves reached the horizontal asymptotic lines, implying that the scour hole was in a relatively stable state. All cases in the present study satisfied the relationship $\theta>\theta_{cr}$, indicating the prevalence of live bed scour; thus, the scour evolution curves fluctuated significantly due to the backfilled effects in the scour hole under a live bed regime (Larsen *et al.*, 2017). The curves continued to fluctuate at the end of experiments, indicating that the equilibrium scour state was not reached in accordance with the equilibrium criterion proposed by Melville and Chew (1999).

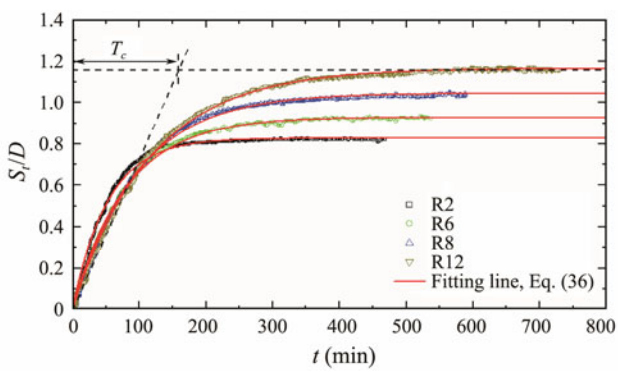

Fig.5 Scour evolution curves of cases R2, R6, R8, and R12.

Fig.6 shows the scour morphology of case R8 after the waves and currents action for 8 h. An inverted cone scour hole (1.01D in depth and 1.32D in diameter) appears around the pile, and it converges with the result obtained by Qi and Gao (2014) under combined waves and currents.

Fig.6 Scour morphology around a single pile.

2) Scour depth prediction for large-scale model tests

Suppose that $S_{\max}$ stands for the maximum scour depth around a pile. Fig.7 depicts the experimental results in $\log(S_{\max})-\log(\lambda_h)$ coordinate. The red line in Fig.7 presents the fitting results of small-scale model tests ($\lambda_h<45$), and the fitting variance R^2 is 0.998, indicating that $\log(S_{\max})$

and log(λ_h) conformed to a linear relationship, consistent with the result of Eq. (35). Then, the fitting line was used to predict the results of large-scale model tests (λ_h>45), and Fig.7 shows the comparison between the predicted values and experimental data. From Fig.7, the fitting line slightly overestimated the experimental data of large-scale model tests. The maximum error between the predicted values and experimental data was 4.1% when λ_h=25, and the errors can be accepted. However, the errors enlarged with the increase in λ_h. The large-scale model tests conducted were insufficient due to the limitation of the experimental setup. However, further checking for the accuracy of Eq. (35), adequately large-scale model tests are necessary for future studies.

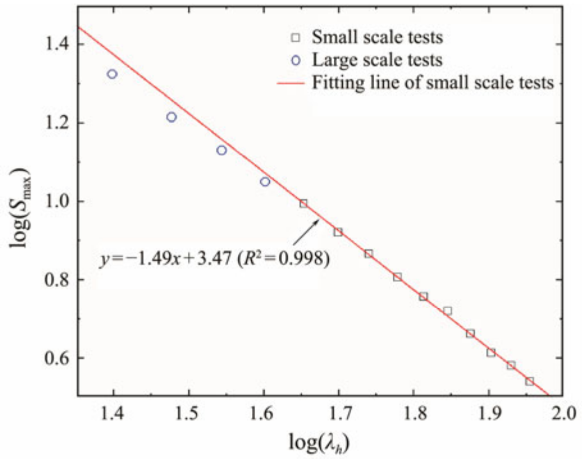

Fig.7 Experimental data of the S_{max} around pile and fitting results of small-scale model tests.

To validate the accuracy of Eq. (35) for predicting the equilibrium scour depth of large-scale model tests, we obtained the equilibrium scour depth S_{eq} by fitting the scour evolution curves using Eq. (36), which was proposed by Sumer and Fredsøe (2002).

$$\frac{S_t}{D}=\frac{S_{eq}}{D}\left(1-\exp\left(\frac{-t}{T_c}\right)\right), \qquad (36)$$

where T_c is the time scale of scour process. T_c defined in Eq. (36) stands for the period when the line passing through the origin of coordinates is tangent to the asymptotic line of S_t/D (Fig.5).

Fig.5 shows the fitting results of Eq. (36) of cases R2, R6, R8, and R12 at position S2. The results indicate that Eq. (36) can depict the scour evolution effectively. Fig.8 illustrates the results in log(S_{eq})−log(λ_h) coordinate. S_{eq} in Fig.8 was derived from position S2 (Fig.1). The red line in Fig.8 represents the fitting results of small-scale model tests (λ_h<45), and the fitting variance R^2 was 0.996, indicating that log(S_{eq}) and log(λ_h) conformed to a linear relationship. Therefore, Eq. (37) can be inferred reasonably from Eq. (35).

$$\log S_{eq,m}=C_7-C_8\log\lambda_h\,, \qquad (37)$$

where C_7 and C_8 were constants.

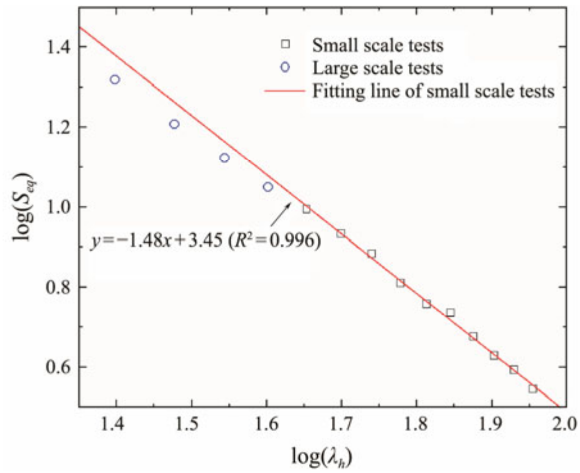

Fig.8 Experimental data of the S_{eq} around the pile and fitting results of small-scale model tests.

The fitting line was used to predict the results of large-scale model tests (λ_h>45), and the comparison between the predicted values and experimental data is shown in Fig.8. As shown in Fig.8, the fitting line slightly overestimated the experimental data of large-scale model tests. The maximum error between the predicted values and experimental data was 4.6% when λ_h=25, and the error can be accepted.

4.2 Tripod

1) Scour evolution and scour morphology

Fig.9 depicts the scour evolution curves of cases R17, R19, and R21 under the main column. As shown in Fig.9, the scour depth increased rapidly at the initial stage, and the scour reached a relatively stable stage. The curves continually fluctuated in all processes due to the passage of sand ripples through the scour hole under the live bed scour regime (Larsen *et al.*, 2017).

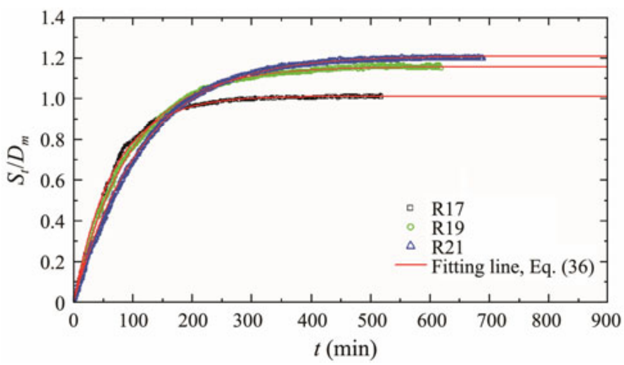

Fig.9 Scour evolution curves of cases R17, R19, and R21.

Given the sufficiently large distance (about 10 D_p, with D_p as the diameter of the tripod's pile) between the adjacent tripod's pile, the group effects on scour can be ignored in accordance with the work of Sumer and Fredsøe (1998). The main column and structural elements have a major effect on the flow field around the tripod. Thus, a special scour morphology can be expected. Fig.10 shows the scour morphology of cases R17, R19, and R21, corresponding to the installation angles of 0˚, 90˚, and 180˚, respectively.

The scour morphology in Fig.10 indicates that the maximum scour hole appeared under the main column in three installation angles in combined waves and current. Moreover, local detached scour holes were present around the tripod's piles. A similar scour morphology was reported by Stahlmann (2013) for tripods and Welzel *et al.* (2019) for jacket structures. In the following section, the maximum and equilibrium scour depths under the main column were selected to evaluate the accuracy of Eqs. (35) and (37) for tripod foundation, respectively.

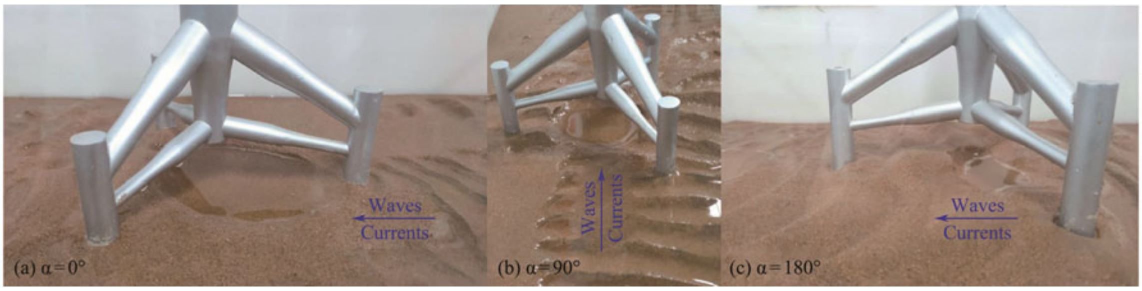

Fig.10 Scour morphology around the tripod: (a) case R17, $\alpha=0°$; (b) case R17, $\alpha=90°$, and (c) case R17, $\alpha=180°$.

2) Scour depth prediction for large-scale model tests

Suppose that $S_{m,\max}$ stands for the maximum scour depth under the main column. Fig.11 presents the experimental data. The red lines in Fig.11 are the fitting results of small-scale model tests ($\lambda_h<45$). The fitting variance R^2 was in the range of 0.994 to 0.996, indicating a linear relationship between $\log(S_{m,\max})$ and $\log(\lambda_h)$. The fitting lines were adopted to predict the results of large-scale model tests ($\lambda_h>45$), and the comparison between the predicting values and experimental data is shown in Fig.11. The comparison showed that the fitting lines slightly overestimated the values of the maximum scour depth of large-scale model tests. The maximum error between the predicted values and experimental data was 6.7% when $\lambda_h=30$ and $\alpha=90˚$, and the error can be accepted. In general, Eq. (35) was applied to the foundation with a complex shape, *e.g.*, the tripod foundation. However, as described above, the errors enlarged with the increase in λ_h. Thus, further validation for the accuracy of Eq. (35) for adequately large-scale model tests is necessary for future studies.

To validate the accuracy of Eq. (37) for predicting the equilibrium scour depth of large-scale model tests for tripod foundation, we obtained the equilibrium scour depth $S_{m,eq}$ by fitting the scour evolution curves using Eq. (36), which was proposed by Sumer and Fredsøe (2002). Fig.12 shows the values of the equilibrium scour depth around tripod foundation in three installation angles. The red lines in Fig.12 are the fitting results of small-scale model tests ($\lambda_h<45$), with the fitting variance R^2 in the range of 0.992 to 0.998. The fitting lines were used to predict the results of large-scale model tests ($\lambda_h>45$), and the comparison between the predicted values and experimental data is shown in Fig.12. Fig.12 displays that the fitting lines caused relatively larger values of $S_{m,eq}$ than the experimental results of large-scale model tests. The maximum error between the predicted values and experimental data was 6.2% when $\lambda_h=30$ and $\alpha=90˚$, and the error can be accepted. Overall, Eq. (37) was also applied to the foundation with a complex shape, *e.g.*, the tripod foundation.

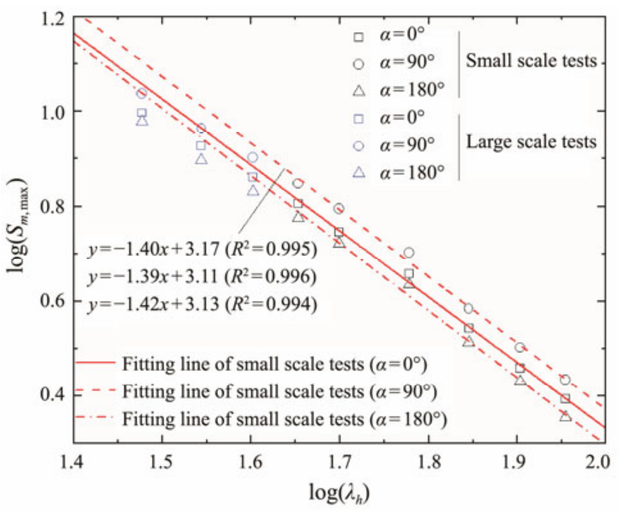

Fig.11 Experimental data of the $S_{m,\max}$ around tripod and fitting results of small-scale model tests.

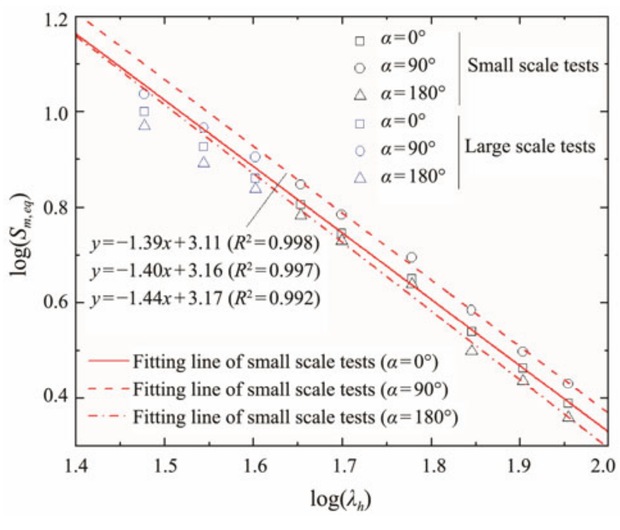

Fig.12 Experimental data of the $S_{m,eq}$ around the tripod and fitting results of small-scale model tests.

5 Discussion

In this study, an innovative theoretical approach was proposed to predict the scour depth around foundations in large-scale model tests based on small-scale model tests under combined waves and currents. In the present approach, the hydrodynamic parameters were designed based on Froude similitude criteria. According to published literature (Ettma *et al.*, 1998; Lee and Sturm, 2009; Schendel *et al.*, 2018; Wu *et al.*, 2020), scaling the sediment median diameter d_{50} based on geometric similarity, *i.e.*, $\lambda_{d_{50}}=\lambda_h$, will lead to a very small model sediment size, exhibiting cohesive behavior. Moreover, preparing materials with very small particle sizes for small-scale model tests is difficult. Thus, a new approach was proposed to select the sediment size in model tests. In the present approach, the sediment size was scaled based on the settling velocity similarity, *i.e.*, the suspended load similarity. In the experimental section, a series of different scale model tests was conducted to verify the correctness and accuracy of Eqs. (35) and (37) for the single pile and tripod foundation. Eqs. (35) and (37) were applied to predict the maximum or equilibrium scour depth in large-scale model tests around a single pile and tripod. According to Eqs. (35) and (37), the maximum or equilibrium scour depth in large-scale tests can be obtained by the fitting line from the results of small-scale tests. Theoretically, the maximum or equilibrium scour depth in the prototype can also be acquired by extending the fitting line to $\log(\lambda_h)=0$. In the present study, the large-scale model tests were insufficient due to the limitation of the experimental setup. Thus, the accuracy of Eqs. (35) and (37) were only validated in limited large-scale tests, with values of $\lambda_h=25-40$ for single piles and $\lambda_h=30-40$ for tripods. Thus, further checks for the accuracy of Eqs. (35) and (37) for a large-scale model or field tests are necessary for future studies. As reported by Sutherland and Whitehouse (1998), ensuring the bedload and suspended load similarity simultaneously in model tests is impossible, but the model should have the same dominant sediment transport mode as the prototype. The sediment size was scaled based on the suspended load similarity in the present approach. Thus, the prerequisite for the application of the present approach is the suspended load dominating the sediment transport in the prototype.

The KC and U_{cw} are directly related to scour depth around foundations in combined waves and currents (Sumer and Fredsøe, 2001; Qi and Gao, 2014; Yu *et al.*, 2020). In the present approach, the hydrodynamic parameters correspond to the Froude similarity criteria from the prototype to the model, and the dimensions of single piles and tripods were scaled based on geometric similarity, which ensured that the KC and U_{cw} were the same in different scale model tests. As described above, the choice of sediment size in the model distorted the geometric similarity, leading to the variation in θ and θ_{cr} in different scale model tests. Although the live bed scour regime was satisfied in all model tests, errors still existed due to the difference in θ and θ_{cr}. Moreover, the disproportionally scaled sediments presumably resulted in the error of bed roughness between the model and prototype, thus causing evident effects on the wave-current boundary layer and scour evolution (Huang *et al.*, 2009; Lee and Sturm, 2009).

Incipient motion occurs when the shear stress τ exerting on the soil particles is greater than the critical threshold shear stress τ_{cr}. Soil particles will suffer from the upward seepage force due to the pressure gradient in the seabed at the wave trough (Jeng, 2013; Xu *et al.*, 2019; Hu *et al.*, 2020; Ren *et al.*, 2021), contributing to the onset of sediment motion; however, the pressure gradient cannot be scaled exactly in the model. Moreover, extensive studies have demonstrated that the horseshoe and wake vortexes are responsible for scour around foundations, and Froude number F_r and pile Reynolds number Re_d have significant effects on the intensity and scale of horseshoe vortex (Sumer *et al.*, 1997; Roulund *et al.*, 2005; Qi and Gao, 2014; Tavouktsoglou *et al.*, 2017; Corvaro *et al.*, 2018). High F_r and Re_d lead to a stagnation point at the upstream foundation edges closer to the water surface, and therefore, the intensive horseshoe vortexes emerge. As discussed by Ettema *et al.* (1998) and Corvaro *et al.* (2018), the effects of Re_d can be neglected when the flow around the foundation is fully turbulent, reaching a sufficiently high Re_d and condition of fully turbulent flow in laboratory model tests is difficult.

As for the submarine pipeline, the onset of scour is mainly related to the seepage flow in the seabed beneath the pipeline, which is driven by the pressure difference between the upstream and downstream sides of the pipe (Yang *et al.*, 2012a, 2012b). In addition, the vortexes in the vicinity of the pipeline contribute to the scour process by dragging sediments away from the seabed (Yang *et al.*, 2014). For fixed foundations (*e.g.*, single piles and tripods), the horseshoe and wake vortexes cause scour. Therefore, the main mechanism for scour between the fixed foundation and pipeline is discrepant. Thus, the adaptation of the present theoretical approach for submarine pipeline still needs to be further verified, especially in future studies.

In summary, ensuring a rigorous similarity of all parameters between the model and prototype is impossible, which results in errors due to scale effects. The contribution of the present approach lies primarily in the prediction for the maximum or equilibrium scour depth around foundations in large-scale model tests based on small-scale model tests under combined waves and currents. Through the comparison between predicted values and experimental data, the errors of the present approach can be accepted.

6 Conclusions

This study presented an innovative theoretical approach to predicting the scour depth around a foundation in large-scale model tests based on small-scale model tests under combined waves and currents. Then, a series of different scale model tests was conducted to obtain the scour depth around a single pile under combined waves and currents. The accuracy of the present approach was validated by comparing the predicted values with experimental data from large-scale tests. Moreover, the accuracy of the present approach for foundations with complex shapes, *e.g.*, the tripod foundation, was further checked. Finally, the merits and disadvantages of the present approach were evaluated in the discussion section. The main conclusions can be described as follows.

1) The contribution of the present approach lies primarily in the prediction for the maximum or equilibrium scour depth around foundations in large-scale model tests based on small-scale model tests under combined waves and currents.

2) In the present approach, the hydrodynamic parameters in the model tests were designed based on Froude similitude criteria. To avoid the cohesive behavior, we scaled the sediment size based on the settling velocity similarity, *i.e.*, the suspended load similarity.

3) The fitting line of small-scale model tests slightly overestimated the experimental results of large-scale model tests. The maximum errors between the predicted values and experimental data were 4.1% and 6.7% for single pile and tripod, respectively, and the errors can be accepted. Therefore, the present approach was applied to predict the maximum or equilibrium scour depth of the large-scale model tests around single piles and tripods.

4) The accuracy of the present approach was validated only in limited large-scale tests, $\lambda_h=25-40$ for single piles and $\lambda_h=30-40$ for tripods. However, further checks for the accuracy of the present approach for sufficient large-scale model tests or field tests are necessary for future studies.

Acknowledgements

This work was financially supported by the Fundamental Research Funds for the Central Universities (No. 2020610 27), and the National Natural Science Foundation of China (No. 41572247).

References

Arboleda Chavez, C. E., Stratigaki, V., Wu, M., and Troch, P. D., 2019. Large-scale experiments to improve monopile scour protection design adapted to climate change–The PROTEUS project. *Energies*, **12** (9): 1-25.

Corvaro, S., Marini, F., Mancinelli, A., Lorenzoni, C., and Brocchini, M., 2018. Hydro- and morpho-dynamics induced by a vertical slender pile under regular and random waves. *Journal of Waterway Port Coastal and Ocean Engineering*, **144** (6): 04018018.

Engelund, F., and Hansen, E., 1967. A monograph on sediment transport in alluvial streams. *Hydraulic Engineering Reports*. Technical University of Denmark, Copenhagen, Denmark.

Ettema, R., Melville, B., and Barkdoll, B., 1998. Scale effect in pier-scour experiments. *Journal of Hydraulic Engineering*, **124**: 639-642.

Fazeres-Ferradosa, T., Chambel, J., Taveira-Pinto, F., Rosa-Santos, P., Taveira-Pinto, F. V. C., Giannini, G., *et al.*, 2021. Scour protections for offshore foundations of marine energy harvesting technologies: A review. *Journal of Marine Science and Engineering*, **9** (3): 1-35.

Fazeres-Ferradosa, T., Taveira-Pinto, F., Romão, X., Reis, M., and Neves, L. D., 2019. Reliability assessment of offshore dynamic scour protections using copulas. *Wind Engineering*, **43** (5): 506-538.

Hu, R. G., Liu, H. J., Leng, H., Yu, P., and Wang, X. H., 2021. Scour characteristics and equilibrium scour depth prediction around umbrella suction anchor foundation under random waves. *Journal of Marine Science and Engineering*, **9** (8):1-35.

Hu, R. G., Yu, P., Wang, Z. Y., Shi, W., and Liu, H. J., 2020. Pore pressure response and residual liquefaction of two-layer silty seabed under standing waves. *Ocean Engineering*, **218**: 108176.

Huang, L. C., and Xu, G. X., 2008. *Hydraulic and River Model Test*. The Yellow River Conservancy Press, Zhengzhou, 1-253 (in Chinese).

Huang, W., Yang, Q., and Xiao, H., 2009. CFD modeling of scale effects on turbulence flow and scour around bridge piers. *Computers and Fluids*, **38** (5): 1050-1058.

Jeng, D. S., 2013. *Porous Models for Wave-Seabed Interactions*. Shanghai Jiao Tong University Press, Shanghai, 1-290.

Jia, Y. G., Liu, X. L., Zhang, S. T., Shan, H. X., and Zheng, J., 2020. *Wave-Forced Sediment Erosion and Resuspension in the Yellow River Delta*. Shanghai Jiao Tong University Press, Shanghai, 1-303.

Larsen, B. E., Fuhrman, D. R., Baykal, C., and Sumer, B. M., 2017. Tsunami-induced scour around monopile foundations. *Coastal Engineering*, **129**: 36-49.

Le Roux, J. P., 2001. A simple method to predict the threshold of particle transport under oscillatory waves. *Sedimentary Geology*, **143** (1): 59-70.

Lee, S. O., and Sturm, T. W., 2009. Effect of sediment size scaling on physical modeling of bridge pier scour. *Journal of Hydraulic Engineering*, **135** (10): 793-802.

Li, H., Ong, M. C., Leira, B. J., and Myrhaug, D., 2018. Effects of soil profile variation and scour on structural response of an offshore monopile wind turbine. *Journal of Offshore Mechanics and Arctic Engineering*, **140**: 042001.

Li, S. Q., 2016. *Sediment Movement in Wave-Current Boundary*. Hohai University Press, Nanjing, 1-157 (in Chinese).

Melville, B. W., and Chiew, Y. M., 1999. Time scale for local scour in bridge piers. *Journal of Hydraulic Engineering*, **125**: 59-65.

Petersen, T. U., Sumer, B. M., and Fredsøe, J., 2012. Time scale of scour around a pile in combined waves and current. *The Proceedings of the 6th International Conference on Scour and Erosion*. Paris, 27-31.

Qi, W. G., and Gao, F. P., 2014. Physical modeling of local scour development around a large-diameter monopile in combined waves and current. *Coastal Engineering*, **83**: 72-81.

Ren, Y. P., Zeng, Y., Xu, X. B., and Xu, G. H., 2021.Sedimentary changes of a sand layer in liquefied silts. *Journal of Ocean University of China*, **20** (5): 1046-1054.

Roulund, A., Mutlu Sumer, B., Fredsøe, J., and Michelsen, J., 2005. Numerical and experimental investigation of flow and scour around a circular pile. *Journal of Fluid Mechanics*, **534**: 351-401.

Schendel, A., Hildebrandt, A., Goseberg, N., and Schlurmann, T., 2018. Processes and evolution of scour around a monopile induced by tidal currents. *Coastal Engineering*, **139**: 65-84.

Schendel, A., Welzel, M., Schlurmann, T., and Hsu, T. W., 2020. Scour around a monopile induced by directionally spread irregular waves in combination with oblique currents. *Coastal Engineering*, **161**: 103751.

Simons, R., Myrhaug, D., and Thais, L., 2001. Bed friction in combined wave-current flows. *The Proceedings of the 27th In-*

ternational Conference on Coastal Engineering. Sydney, 216-226.

Stahlmann, A., 2013. Experimental and numerical model of scour at offshore wind turbines. PhD thesis. Franzius-Institute for Hydraulic, Estuarine and Coastal Engineering. Leibniz Universität Hannover, Hannover, Germany.

Sumer, B. M., and Fredsøe, J., 1998. Wave scour around group of vertical piles. *Journal of Waterway, Port, Coastal, and Ocean Engineering*, **124** (5): 248-256.

Sumer, B. M., and Fredsøe, J., 2001. Scour around pile in combined waves and current. *Journal of Hydraulic Engineering*, **127** (5): 403-411.

Sumer, B. M., Christiansen, N., and Fredsøe, J., 1997. The horseshoe vortex and vortex shedding around a vertical wall-mounted cylinder exposed to waves. *Journal of Fluid Mechanics*, **332**: 41-70.

Sumer, B. M., Fredsøe, J., and Christiansen, N., 1992. Scour around vertical pile in waves. *Journal of Waterway Port Coastal and Ocean Engineering*, **118** (1): 15-31.

Sumer, B., and Fredsoe, J., 2002. Time scale of scour around a large vertical cylinder in waves. *The Proceedings of Kitakyushu.* Japan, 55-60.

Sutherland, J., and Whitehouse, R. J. S., 1998. Scale effects in the physical modelling of seabed scour. *Technical Report.* HR Wallingford, Oxford, UK.

Tavouktsoglou, N. S., Harris, J. M., Simons, R. R., and Whitehouse, R. J. S., 2017. Equilibrium scour-depth prediction around cylindrical structures. *Journal of Waterway, Port, Coastal, and Ocean Engineering*, **143**: 04017017.

Wang, Y. H., Jiang, W. G., and Wang, Y. H., 2013. Scale effects in scour physical-model tests: Cause and alleviation. *Journal of Marine Science and Technology*, **21**: 532-537.

Welzel, M., Schendel, A., Hildebrandt, A., and Schlurmann, T., 2019. Scour development around a jacket structure in combined waves and current conditions compared to monopile foundations. *Coastal Engineering*, **152**: 103515.

Wu, M., De Vos, L., Arboleda Chavez, C. E., Stratigaki, V., Fazeres-Ferradosa, T., Rosa-Santos, P., *et al.*, 2020. Large scale experimental study of the scour protection damage around a monopile foundation under combined wave and current conditions. *Journal of Marine Science and Engineering*, **8** (6): 1-30.

Xu, X. B., Xu, G. H., Ren, Y. P., Liu, Z. Q, and Chen, C. Y., 2019. Horizontal normal force on buried rigid pipelines in fluctuant liquefied silty soil. *Journal of Ocean University of China*, **18** (1): 1-8.

Yang, L. P., Guo, Y. K., Shi, B., Kuang, C. P., Xu, W. L., and Cao, S. Y., 2012a. Study of scour around submarine pipeline with a rubber plate or rigid spoiler in wave conditions. *Journal of Waterway, Port, Coastal, and Ocean Engineering*, **138** (6): 484-490.

Yang, L. P., Shi, B., Guo, Y. K., and Wen, X. Y., 2012b. Calculation and experiment on scour depth for submarine pipeline with a spoiler. *Ocean Engineering*, **55**: 191-198.

Yang, L. P., Shi, B., Guo, Y. K., Zhang, L. X., Zhang, J. S., and Han, Y., 2014. Scour protection of submarine pipelines using rubber plates underneath the pipes. *Ocean Engineering*, **84**: 176-182.

Yu, P., Hu, R. G., Yang, J. M., and Liu, H. J., 2020. Numerical investigation of local scour around USAF with different hydraulic conditions under currents and waves. *Ocean Engineering*, **213**: 107696.

Zhang, K. Y., and Jin, Z. G., 2017. *Fluid Dynamics*. Science Press, Beijing, 1-360 (in Chinese).

Zhao, C. J., and Xu, J., 2009. Study on extension method of series models in bed erosion prediction. *Journal of Waterway and Harbor*, **30** (4): 229-232 (in Chinese with English abstract).

Zhou, Z. L., 2009. *Coastal Dynamics*. 4th edition. China Communication Press, Beijing, 1-252 (in Chinese).

(Edited by Xie Jun)